ChemComm

COMMUNICATION

View Article Online
View Journal | View Issue

Cite this: *Chem. Commun.*, 2025, **61**, 9682

Received 7th April 2025,
Accepted 19th May 2025

DOI: 10.1039/d5cc01951f

rsc.li/chemcomm

Covalent POM–Ir hybrid assemblies: tuning redox properties for light-driven multiple charge accumulation†

Nicolas Queyriaux, ‡[a] Maria Wächtler, §[bc] Christian Cariño, [d] Sandra Alves,[d] Benjamin Dietzek-Ivanšić, ¶[bc] Vincent Artero, [a] Anna Proust, [d] Murielle Chavarot-Kerlidou *[a] and Guillaume Izzet *[d]

This study reports the synthesis, electrochemical characterization, and photophysical properties of two novel photoactive polyoxometalate (POM)–Ir photosensitizer hybrid assemblies. Under visible light irradiation in the presence of triethylamine and trifluoroacetic acid, the polyoxomolybdate-based dyad photoaccumulates the electrons *via* an efficient intramolecular photoinduced electron transfer process.

Artificial photosynthesis is an innovative approach to tackle the challenge of converting and storing solar energy into fuels and high-value chemicals.[1,2] To achieve this, an artificial photosynthetic device should be able to harvest sunlight, use this energy to separate charges, and carry out redox reactions. However, reactions of interest are multielectronic processes, whereas absorption of one photon intrinsically generates a monoelectronic charge-separated state. Designing photoactive systems that can accumulate the electrons generated from the sequential absorption of several photons thus represents an attractive solution to synchronize the single-electron nature of light-induced processes with multielectronic catalysis for chemical fuel production.[3–5] In that context, polyoxometalates (POMs) have attracted growing attention owing to the exceptional electron reservoir properties of this class of discrete oxoclusters.[6] Over the past years, various examples of photoactive hybrid assemblies covalently linking a POM unit with a molecular photosensitizer have been reported in the literature.[7–12] Upon visible light irradiation in the presence of a sacrificial electron donor, primarily two electrons can be stored on the POM moiety and, in rare cases, these stored electrons can be further used in catalytic processes.[7,11,13] Another remarkable property of POMs is the ability to tune their redox properties, either by varying the nature of the metal centre (*e.g.*, Keggin in the tungstate or molybdate series), or by counter-cation exchange for protons, which in turn assist in the reduction processes.[14,15] We previously reported the synthesis and photophysical properties of a first generation of polyoxotungstate-iridium(III) conjugates; owing to the excellent photophysical properties of the cyclometalated Ir center (*i.e.*, high luminescence and long-lived excited state), photoinduced charge-separated states with lifetimes among the longest ones reported to date (ranging from nanoseconds to hundreds of nanoseconds) were characterized.[10,11] However, these functional architectures suffer from the poor stability in acidic conditions of the pyridylcarboxylate-based ancillary ligand. In this study, we report a new generation of POM–Ir hybrids based on a more robust $[Ir(ppy)_2(diimine)]^+$ photosensitizer (diimine = **EPIP** = (ethynylphenyl)-imidazo-1,10-phenanthroline); **Ir-EPIP**[16] in (Fig. 1), and two different Keggin polyanions, a polyoxotungstate and a polyoxomolybdate.

Im-K$^{W}_{Sn}$[Ir] and **Im-K$^{Mo}_{Sn}$[Ir]** were synthesized by a Sonogashira coupling between the alkyne-substituted iridium photosensitizer **Ir-EPIP** and the polyoxotungstate- and polyoxomolybdate-based hybrids bearing an iodoaryl moiety, respectively noted **TBA-K$^{W}_{Sn}$[I]**[17] and **TBA-K$^{Mo}_{Sn}$[I]**[18] (TBA = tetrabutylammonium; Fig. 1). The resulting POM–Ir hybrids being obtained as a mixed TBA and iridium cyclometalated salts at the end of the synthesis, we followed the cation metathesis procedure previously developed for a POM–Ru hybrid to isolate **Im-K$^{W}_{Sn}$[Ir]** and **Im-K$^{Mo}_{Sn}$[Ir]** as 1-butyl-3-methylimidazolium (**Im**) salts. The two bright yellow solids were characterized by ^{1}H and ^{31}P NMR

[a] *Université Grenoble Alpes, CNRS, CEA, IRIG, Laboratoire de Chimie et Biologie des Métaux, F-38054 Grenoble, France. E-mail: murielle.chavarot-kerlidou@cea.fr*
[b] *Institute of Physical Chemistry, Friedrich Schiller University, Lessingstraße 4, 07743 Jena, Germany*
[c] *Department of Functional Interfaces, Leibniz Institute of Photonic Technology, Albert-Einstein-Straße 9, 07745 Jena, Germany*
[d] *Sorbonne Université, CNRS, Institut Parisien de Chimie Moléculaire, IPCM, F-75005 Paris, France. E-mail: guillaume.izzet@sorbonne-universite.fr*

† Electronic supplementary information (ESI) available: Synthetic procedures and characterization, additional electrochemical and spectroscopic data. See DOI: https://doi.org/10.1039/d5cc01951f

‡ Current address: Univ Toulouse, CNRS, LCC, Toulouse, France.
§ Current address: Institute of Physical Chemistry and Kiel Nano, Surface and Interface Science KiNSIS, Christian-Albrechts-Universität zu Kiel, Max-Eyth-Straße 1, 24118 Kiel, Germany.
¶ Current address: Leibniz Institute of Surface Engineering, Permoserstraße 15, 04318 Leipzig, Germany.

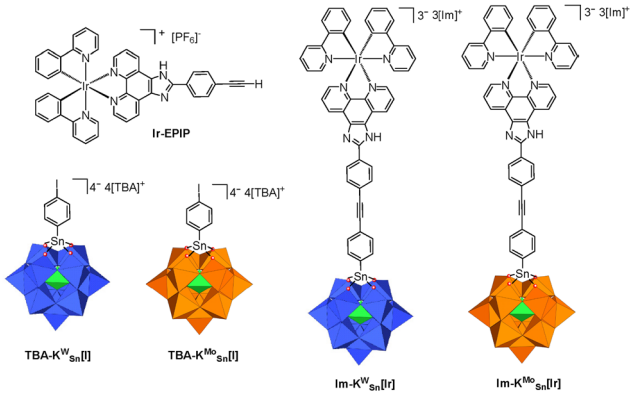

Fig. 1 Structure of **Ir-EPIP**, **TBA-K$^{W}_{Sn}$[I]**, **TBA-K$^{Mo}_{Sn}$[I]** and of the covalent POM–Ir hybrid assemblies **Im-K$^{W}_{Sn}$[Ir]** and **Im-K$^{Mo}_{Sn}$[Ir]** (K^{W}_{Sn} = $[PW_{11}O_{39}Sn]^{4-}$; K^{Mo}_{Sn} = $[PW_{11}O_{39}Sn]^{4-}$; $[TBA]^{+}$ = tetrabutylammonium; $[Im]^{+}$ = 1-butyl-3-methylimidazolium).

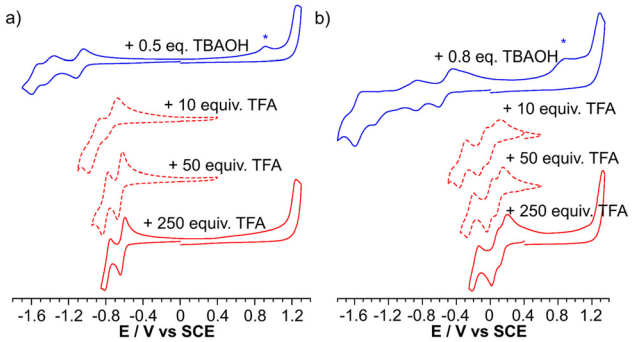

Fig. 2 Cyclic voltammograms of 1 mM solutions of **Im-K$^{W}_{Sn}$[Ir]** (a) and **Im-K$^{Mo}_{Sn}$[Ir]** (b) in DMF containing 0.1 M $TBAPF_6$ (blue curves; neutral imidazole species formed upon addition of TBAOH), and upon the addition of increasing amounts of TFA (red curves). Scan rate: **Im-K$^{Mo}_{Sn}$[Ir]**, 100 mV s^{-1}; **Im-K$^{W}_{Sn}$[Ir]**: 20 mV s^{-1}. The appearance of the irreversible wave at *ca.* +0.9 V *vs.* SCE labelled * is attributed to the presence of methanol that is added with TBAOH to form the deprotonated form of the hybrid.

spectroscopy, FT-IR spectroscopy, elemental analysis, and mass spectrometry (Fig. S1 and S2, ESI†). Elemental analysis, a UV-Vis absorption titration study (Fig. S3, ESI†), and electrochemistry (Fig. S5, ESI†) were consistent with a partial protonation of the imidazole unit in these hybrids (50% for **Im-K$^{W}_{Sn}$[Ir]** and 80% for **Im-K$^{Mo}_{Sn}$[Ir]**).

The **Ir-EPIP** precursor displays an irreversible anodic wave at +1.32 V *vs.* SCE, attributable to the oxidation of the Ir-phenylpyridine moieties, and a reversible cathodic process at −1.55 V *vs.* SCE (Fig. S4, ESI†). After the addition of 1 equiv. of trifluoroacetic acid (TFA), this wave shifts to −1.28 V *vs.* SCE; this indicates that the first reduction of the iridium complex occurs on the imidazo-phenanthroline ligand, with the waves at −1.28 V and −1.55 V *vs.* SCE corresponding to its protonated and neutral forms, respectively. Regarding the POM–Ir hybrids, **Im-K$^{W}_{Sn}$[Ir]** and **Im-K$^{Mo}_{Sn}$[Ir]** were treated with 0.5 and 0.8 equiv. of TBAOH, respectively, to ensure that they remain in solution exclusively in their neutral imidazole form (Fig. S5, ESI†). Both hybrids display a similar irreversible anodic process at *ca.* +1.30 V attributed to the oxidation of the iridium chromophore. In the reduction part, **Im-K$^{W}_{Sn}$[Ir]** displays three reversible waves at −1.08 V, −1.42 V, and −1.55 V *vs.* SCE, respectively attributed to the two first monoelectronic reductions of the polyoxotungstic framework and the iridium centered process (Fig. 2a). The progressive addition of TFA (10 to 250 equiv.) to the solution of **Im-K$^{W}_{Sn}$[Ir]** results in a continuous shift of the reduction potentials to more positive values, due to proton-assisted electron transfers, as well as an increase in the wave intensities, characteristic of the transition to multielectronic processes and leading to two reversible bielectronic reductions on the POM moiety. This behaviour is well illustrated in the POM chemistry.[14,19] Of note, in the presence of TFA, the electrochemical windows are narrower (owing to the presence of an electrocatalytic wave), which prevents scanning down to the reduction centred on the Ir(III) complex.

Conversely, **Im-K$^{Mo}_{Sn}$[Ir]** displays two monoelectronic reduction waves at −0.52 V and −0.86 V *vs.* SCE, followed by an ill-defined reduction process centered on the POM at −1.3 V *vs.* SCE and the reduction of the iridium complex at −1.55 V *vs.* SCE (Fig. 2b and Fig. S6, ESI†). Following the addition of TFA (from 10 to 250 equiv.), three partly resolved waves, attributed to monoelectronic reduction processes on the polyoxomolybdate framework, shift continuously to more positive potentials. However, owing to the higher basicity of the polyoxomolybdate core, this hybrid is much more sensitive to the presence of protons. This shift is much greater than that observed for **Im-K$^{W}_{Sn}$[Ir]** (Table S1, ESI†). Note that we previously reported that, in the presence of TFA, the polyoxomolybdate platform led to bielectronic processes;[18] yet a careful reinvestigation of the cyclic voltammograms indicates that the waves are monoelectronic. The controlled addition of protons thus enables a fine-tuning of the POM first reduction potential over the −1.08 V to −0.62 V *vs.* SCE and −0.52 to +0.15 V *vs.* SCE range for **Im-K$^{W}_{Sn}$[Ir]** and **Im-K$^{Mo}_{Sn}$[Ir]**, respectively.

The luminescence properties of the complex **Ir-EPIP** have been previously reported.[16] In deaerated DMF solution, the complex displays a broad emission spectrum, characteristic of the phosphorescence of cyclometalated Ir complexes (λ_{max} = 588 nm, τ = 560 ns, Fig. S7, ESI†). Surprisingly, the addition of a few equivalents of TFA drastically increases the emission intensity while not modifying the emission features (*i.e.*, same emission wavelength and lifetime, Table S2, ESI†). The hybrids **Im-K$^{W}_{Sn}$[Ir]** and **Im-K$^{Mo}_{Sn}$[Ir]** display emission spectra similar to that of **Ir-EPIP**. However, while the intensity and lifetime of **Im-K$^{W}_{Sn}$[Ir]** and **Ir-EPIP** are almost identical (in the presence of 10 equiv. TFA), a considerable emission quenching is observed for **Im-K$^{Mo}_{Sn}$[Ir]** (τ = 60 ns, Fig. 3). Note that the luminescence intensity for **Im-K$^{Mo}_{Sn}$[Ir]** slightly increases up to 3 equiv. TFA, followed by a decrease upon further addition of TFA. This suggests that a photoinduced intramolecular electron transfer process from the excited Ir photosensitizer to the appended POM occurs in the polyoxomolybdate hybrid (*i.e.*, oxidative quenching of the Ir excited state, a quenching mechanism by energy transfer being ruled out because of the absence of any significant spectral overlap). The driving force for such a process can be calculated using the Rehm–Weller equation (neglecting

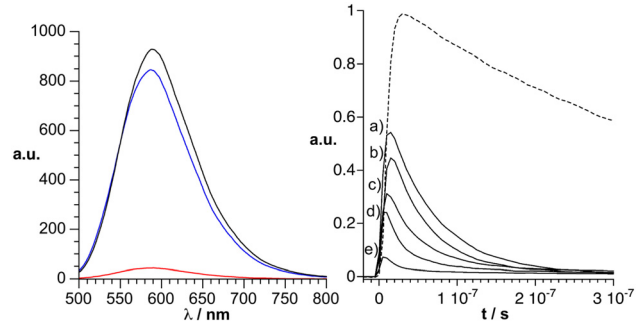

Fig. 3 Left: Luminescence spectra (λ_{exc} = 410 nm) of **Ir-EPIP** (black), **Im-K$^{W}_{Sn}$[Ir]** (blue), and **Im-K$^{Mo}_{Sn}$[Ir]** (red) recorded in DMF (30 μM) in the presence of few equiv. TFA (**Ir-EPIP** and **Im-K$^{W}_{Sn}$[Ir]**: 10 equiv., **Im-K$^{Mo}_{Sn}$[Ir]**: 3 equiv.). Right: Comparison of the emission decay (λ = 590 nm) of **Ir-EPIP** (dotted line) with that of **Im-K$^{Mo}_{Sn}$[Ir]** upon the addition of TFA: (a) 0 equiv.; (b) 10 equiv.; (c) 25 equiv.; (d) 100 equiv., (e) 500 equiv. Note that the intensity scale between **Ir-EPIP** and **Im-K$^{Mo}_{Sn}$[Ir]** does not illustrate the emission quenching.

the electrostatic term);[20] for **Im-K$^{W}_{Sn}$[Ir]** and **Im-K$^{Mo}_{Sn}$[Ir]**, the driving forces of the intramolecular electron transfer are estimated to be *ca.* +0.2 and −0.3 eV, respectively, implying that this process is only thermodynamically allowed for **Im-K$^{Mo}_{Sn}$[Ir]**.

As shown above, adding a proton source considerably increases the reducibility of POMs. However, even if the photoinduced electron transfer becomes thermodynamically favourable (∼−0.2 eV), the addition of up to 100 equiv. of TFA to a solution of **Im-K$^{W}_{Sn}$[Ir]** in DMF does not significantly affect its emission features; this implies that no intramolecular photoinduced electron transfer is occurring. We previously observed that the thermodynamic gain in engaging the reduced species into protonation steps is at the expense of the kinetics of charge injection onto the POM, probably because of increased reorganization energy associated with the POM protonation.[21] This may explain the absence of a photoinduced intramolecular electron transfer process in **Im-K$^{W}_{Sn}$[Ir]** in the presence of the acid. Regarding the polyoxomolybdate analogue, the progressive addition of TFA to a deaerated solution of **Im-K$^{Mo}_{Sn}$[Ir]** in DMF significantly decreases the luminescence lifetime and intensity (Fig. 3 and Table S2, ESI†), as also observed in a POM-Bodipy hybrid.[15] Based on these data, the charge separation (CS) rate constant for the intramolecular electron transfer process could be calculated (Table S2, ESI†). It increases from 1.50×10^{7} s^{-1} in the absence of TFA to 3.71×10^{7} s^{-1} in the presence of 250 equiv. of TFA, highlighting an efficient formation of the charge-separated state in **Im-K$^{Mo}_{Sn}$[Ir]**.

As the polyoxomolybdate core of **Im-K$^{Mo}_{Sn}$[Ir]** displays remarkable electron reservoir properties, we studied the ability of this hybrid to perform charge photoaccumulation. We compared it to that of the polyoxotungstate analogue **Im-K$^{W}_{Sn}$[Ir]**. Electronic spectroscopy can easily monitor the reduction of **Im-K$^{Mo}_{Sn}$[Ir]** as, in their reduced forms, POMs display intense d–d and intervalence charge transfer transitions.[22,23] Prior to photolysis, spectroelectrochemical measurements were carried out on the parent **TBA-K$^{Mo}_{Sn}$[I]** to provide the spectroscopic signatures of the successively formed one-, two-, and even three-electron reduced species (Fig. S8 and S9, ESI†). Spectroelectrochemistry performed without TFA (Fig. S8, ESI†) showed that the one-electron-reduced species has a broad absorbance with an ill-defined maximum of around 790 nm. In the presence of a significant excess of TFA (Fig. S9, ESI†), the absorption maximum of the one-electron-reduced species is slightly blue-shifted to 730 nm. Upon further reduction, the two-electron reduced species displays a *ca.* twice intense absorption band at 705 nm. Finally, applying a more cathodic potential (−0.50 V *vs.* SCE), we could observe that the spectral feature of the solution upon further reduction of the 2e^{-} reduced species displays an absorption maximum at 700 nm and an additional band in the 900–950 nm range, which was attributed to the three-electron reduced polyoxomolybdate hybrid.[24]

Photolysis experiments were then carried out under continuous visible light irradiation (λ > 400 nm) in the presence of triethylamine (TEA, 1 M) as the sacrificial electron donor. The evolution of the electronic spectrum of a degassed DMF solution of **Im-K$^{Mo}_{Sn}$[Ir]** (0.2 mM) is shown in Fig. 4. In the absence of TFA, it is characterized by a broad absorption band with a maximum at approximately 790 nm, characteristic of the one-electron-reduced species, developing over 30 min of irradiation. Irradiation on a longer timescale did not induce any additional changes. This indicates that, under these photolytic conditions (no proton source), only a single light-driven reduction can occur on the polyoxomolybdate core.

Under otherwise identical conditions, the presence of the proton source TFA (500 equiv.) leads to drastic modifications of the spectral change during the photolysis. Adding TFA (pK_a = 6.0 in DMF[25]) implies that the primary source of protons under these conditions is the triethylammonium ion (pK_a = 9.2 in DMF[26]). In the initial stages, a broad band with an ill-defined maximum centered around 750 nm develops (Fig. 4, red trace; 10 min irradiation). This spectral feature closely resembles that of the one-electron electrochemically-reduced species in the presence of TFA. Further irradiation tends to sharpen the low energy region of the absorption band, with a maximum centered at 710 nm (Fig. 4, green trace; 30 min irradiation). This value closely matches the maximum absorption of the two-electron electrochemically-reduced species. Finally, under prolonged photolysis, an additional absorption band slowly emerges around 920 nm (Fig. 4, blue trace; 80 min irradiation). Such a feature strongly agrees with the formation of the three-electron reduced

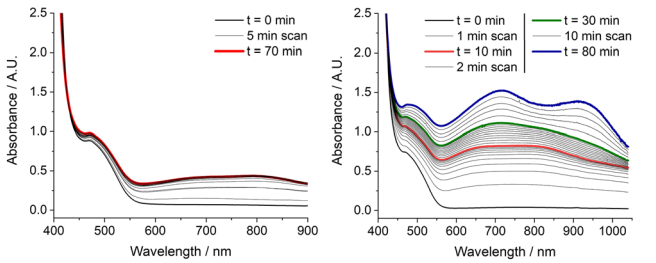

Fig. 4 Evolution of the visible absorption spectrum of a solution of **Im-K$^{Mo}_{Sn}$[Ir]** (0.20 mM) in DMF containing TEA (1 M) under continuous visible light irradiation in the absence (left) and in the presence of 500 equiv. TFA (right).

species, suggesting that upon prolonged irradiation of **Im-K$^{Mo}_{Sn}$[Ir]** in the presence of a proton source—up to three electrons can be stored in the POM scaffold. In sharp contrast, photolysis of the polyoxotungstate analogue **Im-K$^{W}_{Sn}$[Ir]** in the presence of TFA (500 equiv.) did not lead to any spectral changes between 600 and 1000 nm characteristic for the formation of the reduced POM species. Instead, slow accumulation of a new species is observed, tentatively assigned to the reduced [Ir] center[27] formed by TEA's reductive quenching of the Ir excited state (Fig. S10, ESI†). This observation suggests that multiple charge accumulation on the POM moiety can only occur through an intramolecular oxidative quenching process of [Ir]*, followed by its regeneration by TEA. The reasons why thermal electron transfer from the reduced [Ir] center to the polyoxotungstate unit does not occur are still unclear at this stage.

In conclusion, two new **Im-K$^{W}_{Sn}$[Ir]** and **Im-K$^{Mo}_{Sn}$[Ir]** hybrids were electrochemically and spectroscopically characterized, unveiling striking differences in the ability of the photoactive Ir centre to inject charges in the POM moiety, depending on the nature of the metal ion. Moreover, photoirradiation experiments in the presence of a sacrificial electron donor revealed the critical role of adding excess TFA in modulating the photochemical reactivity of **Im-K$^{Mo}_{Sn}$[Ir]** toward multiple charge accumulation. This photoactive hybrid assembly is one of the rare examples of POM-based systems capable of storing more than two electrons under visible light irradiation,[13,28] marking a significant step forward towards their application in challenging multielectron catalytic processes.

This work was supported by the French National Research Agency (Labex ARCANE, CBH-EUR-GS, ANR-17-EURE-0003; and under the France 2030 programme for the PEPR LUMA with the reference ANR-23-EXLU-0001, SYNFLUX-LUMICALS), and the German Science Foundation *via* the Transregio 234 CataLight (project A1, project number 364549901). Dr Martin Schulz is acknowledged for his help in preparing the emission lifetime measurements.

Data availability

The data supporting this article have been included in the ESI.†

Conflicts of interest

There are no conflicts to declare.

Notes and references

1 G. Segev, J. Kibsgaard, C. Hahn, Z. J. Xu, W.-H. Cheng, T. G. Deutsch, C. Xiang, J. Z. Zhang, L. Hammarström, D. G. Nocera, A. Z. Weber, P. Agbo, T. Hisatomi, F. E. Osterloh, K. Domen, F. F. Abdi, S. Haussener, D. J. Miller, S. Ardo, P. C. McIntyre, T. Hannappel, S. Hu, H. Atwater, J. M. Gregoire, M. Z. Ertem, I. D. Sharp, K.-S. Choi, J. S. Lee, O. Ishitani, J. W. Ager, R. R. Prabhakar, A. T. Bell, S. W. Boettcher, K. Vincent, K. Takanabe, V. Artero, R. Napier, B. R. Cuenya, M. T. M. Koper, R. Van De Krol and F. Houle, *J. Phys. D: Appl. Phys.*, 2022, **55**, 323003.
2 S. Berardi, S. Drouet, L. Francas, C. Gimbert-Surinach, M. Guttentag, C. Richmond, T. Stoll and A. Llobet, *Chem. Soc. Rev.*, 2014, **43**, 7501.
3 T. H. Bürgin and O. S. Wenger, *Energy Fuels*, 2021, **35**, 18848.
4 L. Hammarström, *Acc. Chem. Res.*, 2015, **48**, 840.
5 F. Odobel, L. Le Pleux, Y. Pellegrin and E. Blart, *Acc. Chem. Res.*, 2010, **43**, 1063.
6 N. I. Gumerova and A. Rompel, *Nat. Rev. Chem.*, 2018, **2**, 0112.
7 S. Amthor, S. Knoll, M. Heiland, L. Zedler, C. Li, D. Nauroozi, W. Tobaschus, A. K. Mengele, M. Anjass, U. S. Schubert, B. Dietzek-Ivanšić, S. Rau and C. Streb, *Nat. Chem.*, 2022, **14**, 321.
8 F. A. Black, A. Jacquart, G. Toupalas, S. Alves, A. Proust, I. P. Clark, E. A. Gibson and G. Izzet, *Chem. Sci.*, 2018, **9**, 5578.
9 S. Schönweiz, S. A. Rommel, J. Kübel, M. Micheel, B. Dietzek, S. Rau and C. Streb, *Chem. – Eur. J.*, 2016, **22**, 12002.
10 B. Matt, X. Xiang, A. L. Kaledin, N. Han, J. Moussa, H. Amouri, S. Alves, C. L. Hill, T. Lian, D. G. Musaev, G. Izzet and A. Proust, *Chem. Sci.*, 2013, **4**, 1737.
11 B. Matt, J. Fize, J. Moussa, H. Amouri, A. Pereira, V. Artero, G. Izzet and A. Proust, *Energy Environ. Sci.*, 2013, **6**, 1504.
12 F. Odobel, M. Severac, Y. Pellegrin, E. Blart, C. Fosse, C. Cannizzo, C. R. Mayer, K. J. Elliott and A. Harriman, *Chem. – Eur. J.*, 2009, **15**, 3130.
13 W. Wang, L.-M. Chamoreau, G. Izzet, A. Proust, M. Orio and S. Blanchard, *J. Am. Chem. Soc.*, 2023, **145**, 12136.
14 S. Himeno, M. Takamoto, R. Santo and A. Ichimura, *Bull. Chem. Soc. Jpn.*, 2005, **78**, 95.
15 E. Benazzi, J. Karlsson, Y. Ben M'Barek, P. Chabera, S. Blanchard, S. Alves, A. Proust, T. Pullerits, G. Izzet and E. A. Gibson, *Inorg. Chem. Front.*, 2021, **8**, 1610.
16 S. Ramachandra, F. Polo, F. Edafe, K. C. Schuermann, C. A. Nijhuis, P. Belser, W. F. Reus, G. M. Whitesides and L. D. Cola, *Pure Appl. Chem.*, 2011, **83**, 779.
17 B. Matt, J. Moussa, L. M. Chamoreau, C. Afonso, A. Proust, H. Amouri and G. Izzet, *Organometallics*, 2012, **31**, 35.
18 C. Rinfray, S. Renaudineau, G. Izzet and A. Proust, *Chem. Commun.*, 2014, **50**, 8575.
19 S.-X. Guo, A. W. A. Mariotti, C. Schlipf, A. M. Bond and A. G. Wedd, *J. Electroanal. Chem.*, 2006, **591**, 7.
20 $\Delta G \sim E^{*}_{ox} - E_{red} = (E_{ox} - E^{00}) - E_{red}$, with $E_{00} \sim 2.1$ eV for **Ir-EPIP**.
21 C. Rinfray, V. Brasiliense, G. Izzet, F. Volatron, S. Alves, C. Combellas, F. Kanoufi and A. Proust, *Inorg. Chem.*, 2016, **55**, 6929.
22 E. Papaconstantinou and M. T. Pope, *Inorg. Chem.*, 1970, **9**, 667.
23 G. M. Varga, Jr., E. Papaconstantinou and M. T. Pope, *Inorg. Chem.*, 1970, **9**, 662.
24 H.-R. Sun, S.-Y. Zhang, J.-Q. Xu, G.-Y. Yang and T.-S. Shi, *J. Electroanal. Chem.*, 1998, **455**, 57.
25 V. Fourmond, S. Canaguier, B. Golly, M. J. Field, M. Fontecave and V. Artero, *Energy Environ. Sci.*, 2011, **4**, 2417.
26 V. Fourmond, P. A. Jacques, M. Fontecave and V. Artero, *Inorg. Chem.*, 2010, **49**, 10338.
27 J. C. Bawden, P. S. Francis, S. DiLuzio, D. J. Hayne, E. H. Doeven, J. Truong, R. Alexander, L. C. Henderson, D. E. Gómez, M. Massi, B. I. Armstrong, F. A. Draper, S. Bernhard and T. U. Connell, *J. Am. Chem. Soc.*, 2022, **144**, 11189.
28 M. Takahashi, T. Asatani, T. Morimoto, Y. Kamakura, K. Fujii, M. Yashima, N. Hosokawa, Y. Tamaki and O. Ishitani, *Chem. Sci.*, 2023, **14**, 691.